INORGANIC CHEMISTRY FRONTIERS

RESEARCH ARTICLE

View Article Online
View Journal | View Issue

Cite this: *Inorg. Chem. Front.*, 2022, **9**, 2462

$KNa_{0.78}Eu_{0.27}In_{3.80}B_{12}S_{12}$: a novel hexanary thioborate featuring a $B_{12}S_{12}$ cluster and diverse InS_x (x = 4, 5, 6) units†

Shan-Shan Han, Su-Xin Yu, Wenlong Liu and Sheng-Ping Guo *

Received 9th March 2022,
Accepted 13th April 2022

DOI: 10.1039/d2qi00520d

rsc.li/frontiers-inorganic

Thioborates combine the advantages of sulfides and borates, and are a new type of multifunctional inorganic material with versatile structural features. Here, a thioborate $KNa_{0.78}Eu_{0.27}In_{3.80}B_{12}S_{12}$ crystallizing with a new type of compound was synthesized by a high-temperature flux method. Its structure features a rarely discovered $B_{12}S_{12}$ cluster and diverse InS_x (x = 4, 5, 6) units built in a three-dimensional $\{[In_{3.80}B_{12}S_{12}]^{2.6-}\}_\infty$ polyanionic framework. The structural complexity and novelty are well elaborated. Its optical band gap was determined to be 2.28 eV, and a theoretical calculation of its electronic structure was also performed. This work not only enriches the structural chemistry of chalcogenoborates but also provides a new potential RE–B–Q family (RE = rare-earth metal; Q = S, Se). The latter may produce some interesting functionals.

1. Introduction

The boron element features structural complexity, electron deficiency, unusual bonding situations, and builds a rich boron chemistry.[1] Boron and boron-based materials have important applications in modern industry, agriculture, biology, medicine and national defense.[2–8] There are many variants of crystalline elemental boron, and all of them are built by the basic building unit B_{12} icosahedron. Each B_{12} icosahedron has three B–B σ single bonds and ten three-center two-electron (3c–2e) bonds.[9] This specific bonding style yields a rich boron chemistry, in which the *closo*-polyhedral borane anions have drawn attention to these species as precursors of a new and rapidly expanding field of chemistry enriched with novel applications in contemporary materials research.[10–12] *closo*-borane $[B_{12}H_{12}]^{2-}$ is a cluster exhibiting a three-dimensional (3D) aromatic electron delocalization and a remarkable chemical stability.[13–15] In contrast to the highly reactive borane with a small molecular weight, $[B_{12}H_{12}]^{2-}$-based salts are the most stable molecules; this anion survives extended heating in strongly acidic or alkaline solutions.[16,17]

Attracted by the specialty of B_{12}, many efforts have been made to enrich this special entity.[18] Completely saturated with hydrogen, halogens, or even hydroxyl groups, the boron icosahedra can be obtained in solution.[10,19–24] All of these bond with B_{12} to form an anion cluster. Different from this style, B_{12} icosahedron can also connect with twelve Q (Q = S, Se) atoms to form a unique $[B_{12}Q_{12}]^{14-}$ cluster.[25–32] To date, around thirty chalcogenoborates containing $B_{12}Q_{12}$ cluster have been discovered. In their structures, there are two types of coordination environments around each B_{12} icosahedron. One is B_{12} saturated with six BQ_3 units to form the $[B_{12}(BQ_3)_6]^{8-}$ anion,[25] and the other is B_{12} connected with six MQ_4 and two $M'Q_6$ units to build a $[MB_{12}(M'Q_4)_3]^{x-}$ (x = 0, 2; M = Sm, Gd, Ga, In, Sn, Cr; M′ = Ga, In, Sn, Si) open framework.[31,33–37] Specifically, the noncentrosymmetric (NCS) ones of the latter show Kleinman-forbidden second-harmonic generation activity.[33–36]

Chalcogenoborates containing $B_{12}Q_{12}$ clusters are very rare when compared with those containing $B_{12}X_{12}$, $B_{12}(OH)_{12}$ or $B_{12}H_{12}$ clusters.[38–42] Encouraged by the structural diversity for these, it is necessary to explore more $B_{12}Q_{12}$-based ones to enrich their structural chemistry and explore their application potentials. Based on this consideration, our continuous investigation of the $[B_{12}Q_{12}]^{14-}$-based system has led to the discovery of a novel hexanary thioborate, $KNa_{0.78}Eu_{0.27}In_{3.80}B_{12}S_{12}$ (**1**). Its 3D structure features two types of B_{12} icosahedron and diverse InS_x (x = 4, 5, 6) units, and B_{12} icosahedra are consolidated by eight or four InS_x units, representing a new type of chalcogenoborate. Here, the synthesis, crystal structure, and diverse characterizations are reported.

School of Chemistry and Chemical Engineering, Yangzhou University, Yangzhou, Jiangsu 225002, P. R. China. E-mail: spguo@yzu.edu.cn

†Electronic supplementary information (ESI) available: Crystal data tables, crystal photographs, EDS and other tables. CCDC 2086848. For ESI and crystallographic data in CIF or other electronic format see DOI: **https://doi.org/10.1039/d2qi00520d**

2. Experimental section

2.1. Synthesis and analyses

A high-temperature solid-state method was used to synthesize the crystals of $KNa_{0.78}Eu_{0.27}In_{3.80}B_{12}S_{12}$ (**1**). All the starting materials were used as received without further purification. Considerable efforts were devoted to synthesize **1**, and eventually an optimized routine with a high yield was found. For the optimized synthetic route, a 500 mg mixture of Eu_2O_3 (99.9%), In_2O_3 (99.9%), S (99.95%) and B (99%) with 1 : 3 : 16 : 12 of Eu : In : B : S, and an additional 400 mg of NaI and 200 mg of KI (99%) as flux, were used as the starting materials, which were hand-ground in an agate mortar for 30 minutes. The obtained mixture was pressed into a pellet and then loaded into an evacuated quartz ampoule with a vacuum degree of 1×10^{-4} Torr. The quartz tube was put in a muffle furnace and heated to 950 °C in 25 h and kept for 7 days, and then cooled down to 300 °C in 5 days. The dark-red crystals of **1** are stable without any change after exposure to air for a few months at room temperature.

A semiquantitative microscopic elemental analysis on the as-prepared single-crystals of **1** was performed on a field-emission scanning electron microscope (FESEM, Zeiss-Supra55) equipped with an energy dispersive X-ray spectroscope (EDS, Bruker, Quantax), which confirmed the presence of K, Na, Eu, In and S. Specifically, the average ratio of In and Eu is 13, close to that of the single-crystal structure analysis, determined as 14.07. The B element could not be detected in view of its light mass (Table S1 and Fig. S1†).

The inductively coupled plasma (ICP) spectroscopy of **1** was measured on an Optima 7300 DV spectrometer. Polytetrafluoroethylene(PTFE) beakers were used to dissolve the powder of **1** and blank samples were also measured to eliminate background effects. The results show that the mass ratios of Eu/In (14.67) and K/Na (1.26) are close to the theoretical values (Eu/In = 14.07 and K/Na = 1.33).

The powder X-ray diffraction measurement of **1** was carried out with a Bruker D8 Advance diffractometer at 40 kV and 100 mA for Cu-Kα radiation (λ = 1.5406 Å) at room temperature. The 2θ range was 10–60° with a scan step width of 2°. The calculated pattern was generated using the Mercury program with its single-crystal structure data. JANA2006 software was employed to perform the Rietveld refinement (Table S2† and Fig. 1).

2.2. Crystal data

Several suitable single crystals of **1** were selected using an optical microscope for the single-crystal X-ray diffraction analysis. The diffraction data were collected by using a graphite-monochromated Mo-Kα radiation (λ = 0.71073 Å) at room temperature on a Bruker D8 QUEST X-ray diffractometer. The structure was solved by direct methods and refined on F^2 by full-matrix least-squares methods using the Shelxtl2014 crystallographic software package.[43] The crystallographic data are listed in Table 1, and the atom positions and anisotropic displacement parameters (ADP), and bond distances are listed in Tables S3 and S4,† respectively. The CIF document has also been deposited with the CCDC 2086848.†

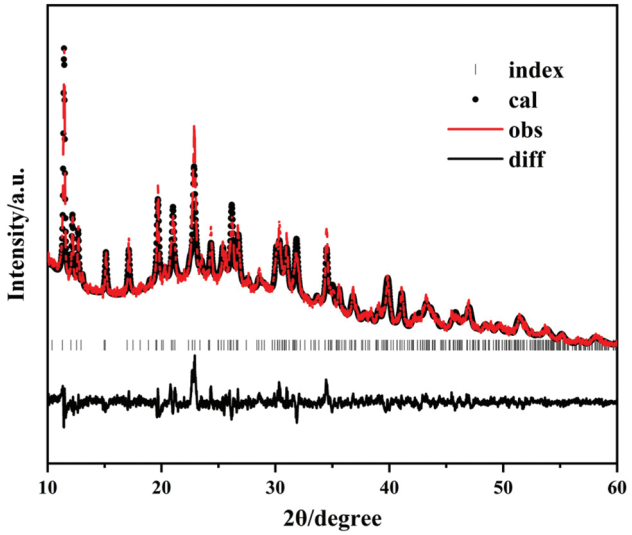

Fig. 1 Rietveld refinement for the powder X-ray diffraction pattern of **1**.

Table 1 Crystal data and structure refinement parameters for **1**

Chemical formula	$KNa_{0.78}Eu_{0.27}In_{3.80}B_{12}S_{12}$
FW	1048.21
T (K)	296
Crystal system	Monoclinic
Space group	$C2/m$
Z	4
a (Å)	15.2538(12)
b (Å)	10.4468(7)
c (Å)	14.6131(10)
β (°)	105.036(3)
V (Å^3)	2248.9(3)
D_{calcd} (g cm^{-3})	3.096
μ (mm^{-1})	5.888
F(000)	1930.0
Crystal size/mm^3	0.136 × 0.12 × 0.05
2θ range (°)	4.78 to 50.942
Indep. reflns./R_{int}	2108/0.0245
Data/restraints/parameters	2108/0/164
GOF on F^2	1.097
$R1^a$ ($I > 2\sigma(I)$)	0.0306
w$R2^b$ (all data)	0.0701

^{a} $R1 = ||F_o| - |F_c||/|F_o|$. ^{b} $wR2 = [w(F_o^2 - F_c^2)^2]/[w(F_o^2)^2]^{1/2}$.

Considering that the structure of **1** is heavily disordered, involving partial occupation and spilt sites, it is necessary to make a detailed description about the structure solution process, which can be described as below. First, the EDS analysis result indicates that K, Na, Eu, In and S are the compositional elements in crystals of **1**, and all these elements have nonnegligible contents according to the EDS analysis of more than 30 single-crystals. Second, all the B, S, and K sites are fully occupied with reasonable anisotropic displacement factors (ADPs). Third, two of the three In sites are fully occupied, while the third one (In(1)) is partially occupied, and the occupancy was freely refined to 0.80. Fourth, the occupancy of

Eu(1) was freely refined to 0.27. Compared with the refinement results for the model with a full occupation of In(1) and Eu(1) atoms, the *R*1 value reduced from 0.1153 to 0.0492. Fifth, the Na(1) site was split over two neighboring sites, namely, Na(1A) on Wyckoff site *m* and Na(1B) on Wyckoff site 2/*m*. The occupancies for these two sites were refined to 0.56 for Na(1A) and 0.44 for Na(1B). The incomplete occupations of Eu and In atoms in other works were also discovered (Table S5†). Combining the above considerations together, the chemical formula of **1** is given as $KNa_{0.78}Eu_{0.27}In_{3.80}B_{12}S_{12}$.

2.3. UV–vis–NIR diffuse reflectance spectroscopy

The UV-vis-NIR diffuse reflection spectrum was recorded at room temperature using a powder $BaSO_4$ sample as a standard on a computer-controlled Cary 5000 UV–vis–NIR spectrometer equipped with a diffuse reflectance accessory at 200–2500 nm. The spectrum was calculated from the reflection spectrum by the Kubelka–Munk function:[44]

$$F(R) = (1-R)^2/(2R) = K/S$$

where R is the reflectance, K is the absorption, and S is the scattering. In the (K/S) *versus* E plot, extrapolating the linear portion of the rising curve to zero gives rise to the onset of absorption.

2.4. Thermal analysis

Differential scanning calorimetry (DSC) analysis on **1** was performed by using a Mettler Toledo thermal analyzer under N_2 atmosphere. The powder sample of **1** was put into a crucible and heated to 1000 °C and cooled back to room temperature at a rate of 10 °C min^{-1}.

2.5. Calculation details

The electronic structure calculation, including band structure and density of states (DOS), was performed using the CASTEP module in Material Studio.[45] A generalized gradient approximation (GGA) by PBE was adopted to describe the exchange–correlation energy. The electronic configurations for In, B, S, Na, K, and Eu were 5s and 5p, 2s and 2p, 3s and 3p, 3s, 4s, 5s/6s and 4f, respectively, and a cutoff energy of 700 eV was set. The numerical integration of the Brillouin zone was implemented by employing 2 × 2 × 4 Monkhorst–Pack *k*-point sampling. The Fermi level at 0 eV was chosen as the reference.

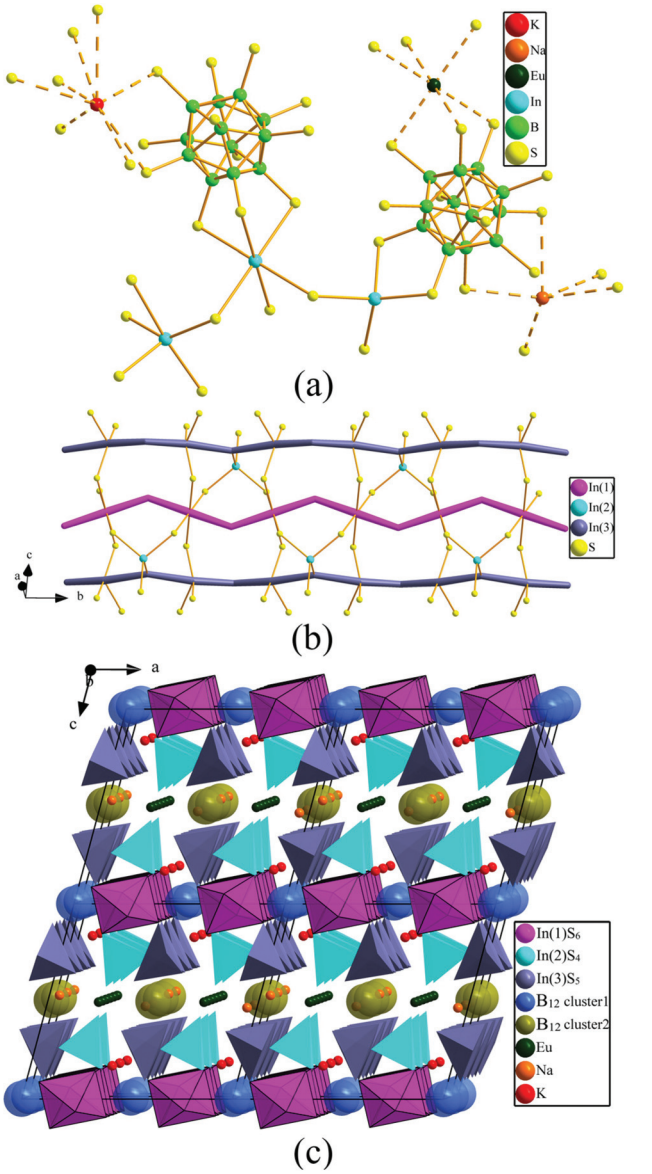

Fig. 2 Crystal structure of **1**: (a) Coordination geometry; (b) $\{[In_{3.80}S_{12}]^{12.6-}\}_\infty$ polyanionic ribbons along the *b* axis; (C) 3*D* view of the crystal structure along the *b* direction.

3. Results and discussion

3.1. Crystal structure

1 adopts a new monoclinic structure type with the space group *C*2/*m* (Pearson code *mC*119.4). There are three In, eight S, eight B, one K, one Na and one Eu sites in the crystallographically independent unit in the structure of **1** (Fig. 2a). Eight kinds of B atoms comprise two types of B_{12} icosahedra. For the sake of clarity, each B_{12} icosahedron is dummied into one sphere. Two B(2), two B(3), four B(4) and four B(7) link together to form a B_{12} icosahedron (type-I) with the B–B distances in the range 1.768(9)–1.806(8) Å. Meanwhile, two B(1), two B(5), four B(6) and four B(8) build a B_{12} (type-II) icosahedron, in which the B–B bond lengths are 1.764(8)–1.805(8) Å. In both cases, there are nine types of B–B distances, showing the B–B bond distance dispersity.

Na, K, and Eu metal elements are surrounded with five, eight, and six S atoms to form a NaS_5 trigonal bipyramid, KS_8 cuboctahedron, and EuS_6 octahedron, respectively. Each B_{12} icosahedron has twelve nearest S atoms to form the $B_{12}S_{12}$ cluster, in which each type-I B_{12} icosahedron is surrounded by two InS_4 tetrahedra and four InS_5 trigonal bipyramids by sharing edges. Whereas each type-II B_{12} icosahedron is surrounded by four InS_6 octahedra through sharing faces, two

InS_4 tetrahedra and four InS_5 trigonal bipyramids by sharing edges. Both types of $B_{12}S_{12}$ cluster are isolated, and they only connect with InS_x polyhedra. The In(1)S_6 octahedra and In(3)S_5 trigonal bipyramids build two types of *zig-zag* chains and then connect with In(2)S_4 tetrahedra to form $\{[In_{3.80}S_{12}]^{12.6-}\}_\infty$ polyanionic ribbons extending along the *b* direction (Fig. 2b), which further connect with two types of B_{12} to build a 3*D* structure (Fig. 2c).

The simplified 3*D* structure graph of **1** viewing along the *b* and *c* directions is depicted in Fig. 3, where K, Na and Eu atoms are omitted for the sake of clarity, and the B_{12} icosahedron, In(1)S_6 octahedra, In(2)S_4 tetrahedra and In(3)S_5 trigonal bipyramid are dummied to one atom, namely *I*-B_{12}, *O*-In(1)S_6, *T*-In(2)S_4, *TP*-In(3)S_5. The connections between the diverse polyhedra can be clearly observed. There are two-types of connections around *I*-B_{12}, one with four *O*-In(1)S_6, four *TP*-In(3)S_5 and two *T*-In(2)S_4, and the other with four *TP*-In(3)S_5 and two *T*-In(2)S_4. The *I*-B_{12} are isolated from each other, and they are connected by InS_x polyhedra. Each *O*-In(1)S_6 is surrounded by two *I*-B_{12}, two *T*-In(2)S_4, and two *TP*-In(3)S_5, while each *T*-In(2)S_4 is surrounded by two *I*-B_{12}, *TP*-In(3)S_5, and two O-In(1)S_6; and each *TP*-In(3)S_5 is surrounded by two I-B_{12}, one *T*-In(2)S_4, and one *O*-In(1)S_6.

Specifically, the coordination diversity of In atoms is fully exhibited in this structure. In(1), In(2) and In(3) atoms coordinate with six, four and five S atoms to form octahedral In(1)S_6, tetrahedral In(2)S_4 and trigonal bipyramidal In(3)S_5 units. The distances from In to the three equatorial and one of the apical S atoms are short (2.4596(14)–2.5778(9) Å); while the distance to the other apical S atom is considerably longer (2.9409(8) Å) (Fig. S2†). This longer In–S distance is comparable with those in $NaIn_3S_5$, $Ba_{18}F_{18}In_8S_{21}$, $Fe_{1.5}Pb_{5.5}In_{10}S_{22}$, $Ca_{0.76}In_{2.84}S_5$ and $La_4Ag_2In_4S_{13}$ (Table S6†). In other In-containing chalcogenides, tetrahedral and octahedral coordination geometries are normally found for the In atom; in contrast, examples of trigonal bipyramidal geometry are very few, including but not limited to γ-In_2Se_3,[46] $Ga_xIn_{2-x}Se_3$,[47] $BaRE_2In_2Q_7$ (Q = S, Se)[48] and $K_5In_3P_6Se_{19}$.[49] In general, a structure containing three In coordination geometries simultaneously is very rare. At present, it's only discovered in $K_5In_3P_6Se_{19}$.[49] Hence, **1** is the first chalcogenoborate and the second chalcogenide containing three InS_x coordination geometries.

When referring to the different In–S polyhedra, the connection between In and S atoms can be described as a highly distorted In(3)S_5 trigonal bipyramid, slightly distorted In(2)S_4 tetrahedron and normal In(1)S_6 octahedron with gradually reduced calculated dipole moments of 18.8529, 9.2955, and 3.9815 D, respectively. They connect with each other to form $\{[In_{3.80}S_{12}]^{12.6-}\}_\infty$ polyanionic ribbons (Fig. 2b), which represent a new In–S slab. Differently, the three $InSe_x$ coordination geometries in $K_5In_3P_6Se_{19}$ are connected with each other by Se(1) atoms to form the $[In_3Se_{13}]^{17-}$ anion (Fig. S2†).[49]

Differently from the arrangement of other $B_{12}Q_{12}$ compounds,[25,34] the $B_{12}S_{12}$ clusters in **1** are arranged in a cubic closest-packed manner with the center to center distance within 8.987 to 11.857 Å (Fig. S3†).[50] The cluster anions exhibit their centers of gravity at the Wyckoff positions 2*a* (for type-I B_{12}) and 2*d* (for type-II B_{12}), with distances of almost 1.7 Å to the twelve boron atoms, providing them an inner diameter of 3.4 Å, which is close to that of other inorganic compounds containing B_{12} clusters (Table 2) and indicates the high stability of B_{12} clusters.

As far as we know, there are two-types of connection around B_{12} icosahedra: one is surrounded by six BS_3 units to form $[B_{12}(BS_3)_6]^{8-}$ polyanion (Fig. 4a), while the other one is connected with two InS_6 and six InS_4 units to construct the $[In_8B_{12}S_{30}]^{26-}$ polyanion (Fig. 4b).[26,35] Different from these two styles, the B_{12} icosahedron in this work adopts a new connection mode with diverse InS_x units to form the $[In_{7.1}B_{12}S_{29}]^{26.7-}$ anion in **1** (Fig. 4c). Among the two known structure types, a family of multinary $(A_3X)[MB_{12}(M'Q_4)_3]$ (A = alkali metal; X = halogen element; M = Ga, In, rare-earth metal; M′ = Ga, In) compounds have the maximum relevance to the structure of

Table 2 Different B_{12} clusters in known chalcogenoborates

Compound	$\bar{d}$ (B–B)/Å	$\bar{d}$ (C–B)/Å	ID	The CE of B_{12}
$K_3Cl[InB_{12}(InSe_4)_3]$[36]	1.79	1.70	3.40	6[$InSe_4$], 4[$InSe_6$]
$Ag_2B_{12}Cl_{12}$[50]	1.78	1.70	3.40	6[$AgCl_6$]
$Sn_4B_{12}Se_{15}$[31]	1.79	1.70	3.40	6[$SnSe_4$], 2[$SnSe_6$]
$Cs_8B_{12}(BSe_3)_6$[25]	1.78	1.70	3.39	6[BSe_3]
1 (type-I B_{12})	1.79	1.71	3.41	4[InS_5], 2[InS_4]
1 (type-II B_{12})	1.79	1.70	3.40	4[InS_6], 2[InS_4], 4[InS_5]

Note: $\bar{d}$ (C–B), ID and CE represent the average values of the B_{12} gravity's center to B atoms, inner diameter of B_{12}, and chemical environments of B_{12}, respectively.

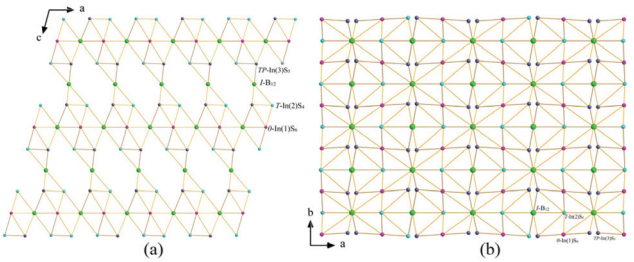

Fig. 3 Simplified open-framework of **1** viewed along the *b* (a) and *c* (b) directions.

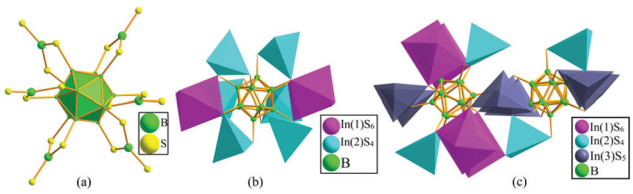

Fig. 4 The chemical environment around one B_{12} icosahedron: $[B_{12}(BS_3)_6]^{8-}$ (a); $[In_8B_{12}S_{30}]^{26-}$ (b); $[In_{7.1}B_{12}S_{29}]^{26.7-}$ (c).

1.[33–36] $(K_3I)[InB_{12}(InS_4)_3]$ crystalizes in the NCS hexagonal space group $P6_322$ featuring a 3D honeycomb-like open-framework, providing channels occupied by face-sharing IK_6 octahedral chains.[35] Accordingly, **1** features $\{[In_{3.80}S_{12}]^{12.6-}\}_\infty$ polyanionic ribbons constructed by diverse InS_x units, which further connect with two types of B_{12} icosahedra to form the 3D structure (Fig. 4c). Unlike **1** with two types of B_{12} icosahedra, $(K_3I)[InB_{12}(InS_4)_3]$ has only one type of B_{12} icosahedron with two unique B atoms, and each B_{12} icosahedron is surrounded by two In(1)S_6 octahedra *via* sharing faces and six In(2)S_4 tetrahedra *via* sharing edges (Fig. 4b and c).

The In(1)–S bond distances in the InS_6 unit are 2.680(6) Å and the In(2)–S bond distances in the InS_4 unit are 2.399(6)–2.492(7) Å in $(K_3I)[InB_{12}(InS_4)_3]$, indicating that In(1)$S_6$ octahedra are normal and centrosymmetric (CS). In(1)S_6 octahedra arrange in a parallel manner and In(2)S_4 tetrahedra settle orderly at a certain angle. Although all the coordination polyhedra in **1** are distorted, it crystallizes in the CS structure, since all the InS_x units in its structure stack in a back-to-back style, which cancels out their hyperpolarizabilities.[51,52] Their NCS/CS structures can also be explained by analyzing their structural symmetry. Considering their unit-cell centers, the In atom coordinates with four S atoms to form a highly distorted InS_4 tetrahedron in $(K_3I)[InB_{12}(InS_4)_3]$ with side lengths of 3.854–4.181 Å, whereas in the symmetric center of **1**, Na and S atoms connect with each other to form two parallelograms with Na–S distances of 3.261(6) and 3.007(5) Å (Fig. 5).

3.2. Optical properties

The optical band gap of **1** was determined to be approximately 2.26 eV from the result of UV-vis-NIR diffuse-reflectance spectroscopy (Fig. 6), which is consistent with its dark-red color.

3.3. Thermal behavior

The differential scanning calorimetry (DSC) result shows that it undergoes melting upon heating and crystallization upon cooling events (Fig. 7).[53,54] The inherently high kinetic stability of the B_{12} icosahedron makes it resistant to decomposition reactions at elevated temperatures, and it is thermally stable up to 739 °C.

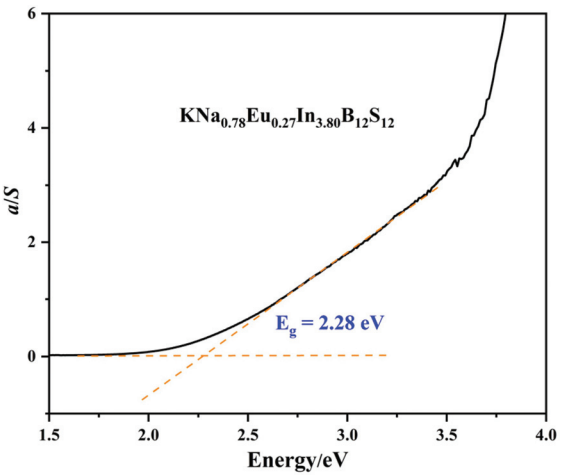

Fig. 6 UV–vis–NIR diffuse reflectance spectrum of **1**.

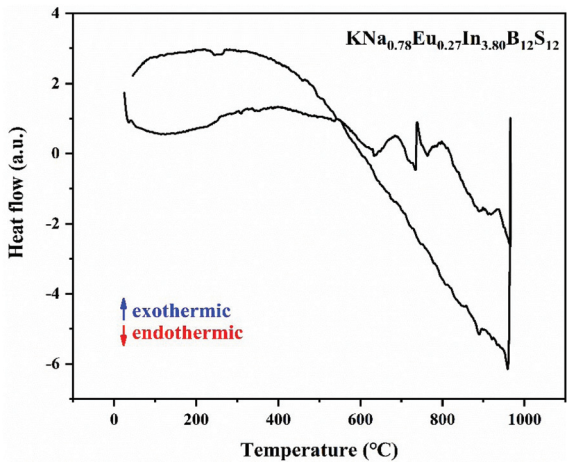

Fig. 7 DSC curve for **1** measured from room temperature to 1000 °C under a N_2 atmosphere.

3.4. Theoretical calculations

To better understand its structure, an electronic structure calculation for **1** was performed. The calculated band gap of **1** is 1.08 eV (Fig. 8a). Usually, the calculated band gap is underestimated compared with its experimental one. The density of

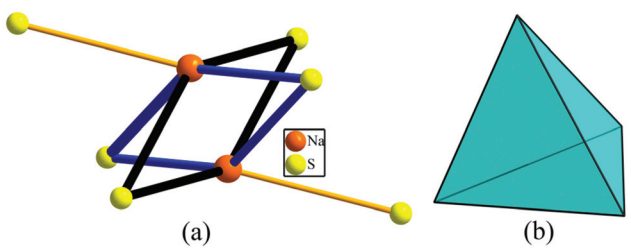

Fig. 5 The center of the unit cell: (a) parallelograms formed by Na and S in 1; (b) highly distorted InS_4 tetrahedron in $(K_3I)[InB_{12}(InS_4)_3]$.

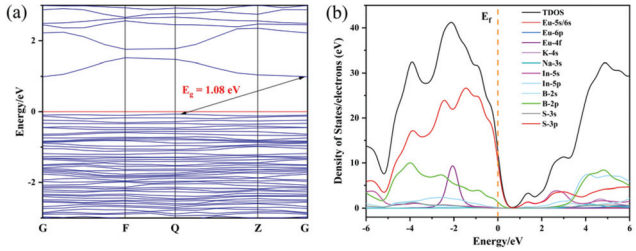

Fig. 8 Calculated electronic structure, including band structure (a) and DOS (b). 0 eV is selected as the Fermi level.

states (DOS) calculation was carried out to observe the orbitals' contribution near the Fermi level (Fig. 8b). Total and Partial DOS show that the top of the valence band is mainly composed of S-3p and minor B-2p orbitals, while the bottom of the conduction band is primarily constituted of In-5s and S-3p orbitals, suggesting that charge transfer between the frontier orbitals is primarily from S 3p to In 5s orbitals. Recalling the case for $(K_3I)[InB_{12}(InS_4)_3]$,[34] similar calculation results are available and also verify that these calculations are reliable.

4. Conclusion

In summary, a novel hexanary thioborate $KNa_{0.78}Eu_{0.27}In_{3.80}B_{12}S_{12}$ (**1**) was obtained and systematically studied. Its structure features an unprecedented $\{[In_{3.80}S_{12}]^{12.6-}\}_\infty$ polyanionic ribbon, two types of B_{12} icosahedra, and diverse InS_x units. **1** is the first thioborate and the second chalcogenide to include InS_4, InS_5 and InS_6 polyhedra in one structure. This work not only provides a novel type of thioborate with a special structure, but also enriches both B and In chemistry. Next, it is proposed to explore its potential structural tolerance for diverse derivatives and physical properties. We hope this work can evoke increasing interest on chalcogenoborates, which really represents an amazing while insufficiently explored material system.

Conflicts of interest

There are no conflicts to declare.

Acknowledgements

The authors would like to acknowledge the financial support by the national natural science foundation of China (21771159, 22071212), and the Qinglan project from Yangzhou University.

References

1 B. Albert and H. Hillebrecht, Boron: Elementary Challenge for Experimenters and Theoreticians, *Angew. Chem., Int. Ed.*, 2009, **48**, 8640–8668.
2 Y. Chi, J. Xu, H. G. Xue, Y. P. Zhang, X. L. Chen, M. H. Whangbo, S. P. Guo and S. Q. Deng, Triple-Kagome-Layer Slabs of Mixed-Valence Rare-Earth Ions Exhibiting Quantum Spin Liquid Behaviors: Synthesis and Characterization of $Eu_9MgS_2B_{20}O_{41}$, *J. Am. Chem. Soc.*, 2019, **141**, 9533–9536.
3 N. S. Hosmane, *Boron Science: New Technologies and Applications*, CRC Press, 2011.
4 Y. Chi, H. G. Xue and S. P. Guo, Designing Sulfide Borate as a Novel Type of Second-Order Nonlinear-Optical Material, *Inorg. Chem.*, 2020, **59**, 1547–1555.
5 Z. H. Zhang, E. S. Penev and B. I. Yakobson, Two-Dimensional Boron: Structures, Properties and Applications, *Chem. Soc. Rev.*, 2017, **46**, 6746–6763.
6 F. Ali, N. S. Hosmane and Y. Zhu, Boron Chemistry for Medical Applications, *Molecules*, 2020, **25**, 828–852.
7 Y. Zhu and N. S. Hosmane, Recent Advances and Applications in Boron Chemistry, *Coord. Chem. Rev.*, 2015, **293**, 357–367.
8 Z. H. Shi, Y. Chi, M. Yang, W. L. Liu and S. P. Guo, A Series of Chalcogenide Borates $RE_6Ta_2MgQB_8O_{26}$ (RE = Sm, Eu, Gd; Q = S, Se) Featuring a B_4O_{10} Cluster, *Inorg. Chem.*, 2020, **59**, 3532–3536.
9 M. Fujimori, T. Nakata, T. Nakayama, E. Nishibori, K. Kimura, M. Takata and M. Sakata, Peculiar Covalent Bonds in α-Rhombohedral Boron, *Phys. Rev. Lett.*, 1999, **82**, 4452–4455.
10 T. Peymann, C. B. Knobler, S. I. Khan and M. F. Hawthorne, Dodecahydroxy-*closo*-Dodecaborate(2−), *J. Am. Chem. Soc.*, 2001, **123**, 2182–2185.
11 O. Conrad, C. Jansen and B. Krebs, Boron-Sulfur and Boron-Selenium Compounds-From Unique Molecular Structural Principles to Novel Polymeric Materials, *Angew. Chem., Int. Ed.*, 1998, **37**, 3208–3218.
12 W. L. Li, X. Chen, T. Jian, T. T. Chen, J. Li and L. S. Wang, From Planar Boron Clusters to Borophenes and Metalloborophenes, *Nat. Rev. Chem.*, 2017, **1**, 0071–0080.
13 M. F. Hawthorne, *Advances in Boron Chemistry: Special Publication No. 201*, Royal Society of Chemistry, London, 1997.
14 J. J. Aihara, Three-Dimensional Aromaticity of Polyhedral Boranes, *J. Am. Chem. Soc.*, 1878, **100**, 3339–3342.
15 R. B. King, Three-Dimensional Aromaticity in Polyhedral Boranes and Related Molecules, *Chem. Rev.*, 2001, **101**, 1119–1152.
16 E. L. Muetterties, J. H. Balthis, Y. T. Chia, W. H. Knoth and H. C. Miller, Chemistry of Boranes. VIII. Salts and Acids of $B_{10}H_{10}^{2-}$ and $B_{12}H_{12}^{2-}$, *Inorg. Chem.*, 1964, **3**, 444–451.
17 A. A. Kamin and M. A. Juhasz, Exhaustive Cyanation of the Dodecaborate Dianion: Synthesis, Characterization, and X-ray Crystal Structure of $[B_{12}(CN)_{12}]^{2-}$, *Inorg. Chem.*, 2020, **59**, 189–192.
18 I. B. Sivaev, V. I. Bregadze and S. Sjöberg, Chemistry of *closo*-Dodecaborate Anion $[B_{12}H_{12}]^{2-}$: A Review, *Collect. Czech. Chem. Commun.*, 2002, **67**, 679–727.
19 T. Peymann, A. Herzog, C. B. Knobler and M. F. Hawthorne, Aromatic Polyhedral Hydroxyborates: Briding Boron Oxides and Boron Hydrides, *Angew. Chem., Int. Ed.*, 1999, **38**, 1061–1064.
20 I. Tiritiris and T. Schleid, Single Crystals of the Dodecaiodo-*closo*-Dodecaborate $Cs_2[B_{12}I_{12}]\cdot 2CH_3CN$ (≡Cs-$(NCCH_3)_2[B_{12}I_{12}]$) from Acetonitrile, *Z. Anorg. Allg. Chem.*, 2001, **627**, 2568–2570.
21 E. V. Bukovsky, D. V. Peryshkov, H. Wu, W. Zhou, W. S. Tang, W. M. Jones, V. Stavila, T. J. Udovic and S. H. Strauss, Comparison of the Coordination of $B_{12}F_{12}^{2-}$, $B_{12}Cl_{12}^{2-}$, and $B_{12}H_{12}^{2-}$ to Na^+ in the Solid State: Crystal

Structures and Thermal Behavior of $Na_2(B_{12}F_{12})$, $Na_2(H_2O)_4(B_{12}F_{12})$, $Na_2(B_{12}Cl_{12})$, and $Na_2(H_2O)_6(B_{12}Cl_{12})$, *Inorg. Chem.*, 2017, **56**, 4369–4379.

22 M. Mayer, M. Rohdenburg, V. van Lessen, M. C. Nierstenhöfer, E. Aprà, S. Grabowsky, K. R. Asmis, C. Jenne and J. Warneke, First Steps Towards a Stable Neon Compound: Observation and Bonding Analysis of $[B_{12}(CN)_{11}Ne]^-$, *Chem. Commun.*, 2020, **56**, 4591–4594.

23 R. T. Boeré, J. Derendorf, C. Jenne, S. Kacprzak, M. Keßler, R. Riebau, S. Riedel, T. L. Roemmele, M. Rühle, H. Scherer, T. Vent-Schmidt, J. Warneke and S. Weber, On the Oxidation of the Three-Dimensional Aromatics $[B_{12}X_{12}]^{2-}$ (X=F, Cl, Br, I), *Chem. – Eur. J.*, 2014, **20**, 4447–4459.

24 H. F. T. Klare and M. Oestreich, Silylium Ions in Catalysis, *Dalton Trans.*, 2010, **39**, 9176–9184.

25 J. Küper, O. Conrad and B. Krebs, Selenoboratoborates $[B_{12}(BSe_3)_6]^{8-}$: A New Class of Chalcogen-Substituted Icosahedral Boron Clusters, *Angew. Chem., Int. Ed. Engl.*, 1997, **36**, 1903–1904.

26 J. Kuchinke, A. Hammerschmidt and B. Krebs, $Rb_8[B_{12}(BS_3)_6]$ and $Cs_8[B_{12}(BS_3)_6]$: The First Thioborato-*closo*-Dodecaborates, *Solid State Sci.*, 2003, **5**, 189–196.

27 A. Hammerschmidt, A. Lindemann, C. Köster and B. Krebs, $Na_6[B_{18}Se_{17}]$: The First Selenoborato-*closo*-Dodecaborate with a Polymeric Chain Anion, *Z. Anorg. Allg. Chem.*, 2001, **627**, 2121–2126.

28 A. Hammerschmidt, A. Lindemann, M. Döch and B. Krebs, A Novel Selenoborato-*closo*-Dodecaborate with Different Anion Substitution Patterns, *Z. Anorg. Allg. Chem.*, 2003, **629**, 1249–1255.

29 A. Hammerschmidt, M. Döch, S. Pütz and B. Krebs, $Na_8[B_{12}(BSe_3)_6]$: A Novel Selenoborato-*closo*-Dodecaborate, *Z. Anorg. Allg. Chem.*, 2004, **630**, 2299–2303.

30 A. Hammerschmidt, M. Döch, S. Pütz and B. Krebs, $Na_2[B_{18}Se_{16}]$: The First 3*D* Polymeric Selenoborato-*closo*-Dodecaborate, *Z. Anorg. Allg. Chem.*, 2005, **631**, 1125–1128.

31 D. G. Chica, I. Spanopoulos, S. Hao, C. Wolverton and M. G. Kanatzidis, $Sn_{4-\delta}B_{12}Se_{12}[Q_x]$, Q = Se, Te, a B_{12} Cluster Tunnel Framework Hosting Neutral Chalcogen Chains, *Chem. Mater.*, 2021, **33**, 1723–1730.

32 A. Hammerschmidt, M. Döch, A. Lindemann, S. Pütz and B. Krebs, Sodium Selenoborato-*closo*-Dodecaborates: Structures and Properties, *Phys. Chem. Glasses: Eur. J. Glass Sci. Technol., Part B*, 2006, **47**, 377–380.

33 S. P. Guo, G. C. Guo, M. S. Wang, J. P. Zou, H. Y. Zeng, L. Z. Cai and J. S. Huang, A Facile Approach to Hexanary Chalcogenoborate Featuring a 3-*D* Chiral Honeycomb-Like Open-framework Constructed from Rare-Earth Consolidating Thiogallate-*closo*-Dodecaborate, *Chem. Commun.*, 2009, 4366–4368.

34 S. P. Guo, Y. Chi, B. W. Liu and G. C. Guo, Synthesis, Crystal Structure and Second-Order Nonlinear Optical Property of a Novel Pentanary Selenide $(K_3I)[InB_{12}(InSe_4)]_3$, *Dalton Trans.*, 2016, **45**, 10459–10465.

35 Z. D. Sun, Y. Chi, H. G. Xue and S. P. Guo, A Series of Pentanary Inorganic Supramolecular Sulfides $(A_3X)[MB_{12}(MS_4)_3]$ (A = K, Cs; X = Cl, Br, I; M = Ga, In, Gd) Featuring $B_{12}S_{12}$ Clusters, *Inorg. Chem. Front.*, 2017, **4**, 1841–1847.

36 S. S. Han, W. D. Yao, S. X. Yu, Y. Sun, A. Gong and S. P. Guo, Salt-Inclusion Chalcogenoborates Containing a $B_{12}Q_{12}$ (Q = S, Se) Cluster Exhibiting a Kleinman-Forbidden Frequency-Doubling Effect, *Inorg. Chem.*, 2021, **60**, 3375–3383.

37 M. Sugimori, H. Fukuoka, H. Imoto and T. Saito, Preparation and Crystal Structure of Chromium Silicon Selenide Containing a B_{12} Icosahedron with a Tunnel Structure, *J. Organomet. Chem.*, 2000, **611**, 547–550.

38 H. Lin, W. B. Wei, H. Chen, X. T. Wu and Q. L. Zhu, Ration Design of Infrared Nonlinear Optical Chalcogenides by Chemical Substitution, *Coord. Chem. Rev.*, 2020, **406**, 213150–213173.

39 M. Y. Ran, Z. J. Ma, H. Chen, B. X. Li, X. T. Wu, H. Lin and Q. L. Zhu, Partial Isovalent Anion Substitution to Access Remarkable Second-Harmonic Generation Response: a Generic and Effective Strategy for Design of Infrared Nonlinear Optical Materials, *Chem. Mater.*, 2020, **32**, 5890–5896.

40 M. M. Chen, Z. Ma, B. X. Li, W. B. Wei, X. T. Wu, H. Lin and Q. L. Zhu, $M_2As_2Q_5$ (M = Ba, Pb; Q = S, Se): A Source of Infrared Nonlinear Optical Materials with Excellent Overall Performance Activated by Multiple Discrete Arsenate Anions, *J. Mater. Chem. C*, 2021, **9**, 1156–1163.

41 H. Chen, W. B. Wei, H. Lin and X. T. Wu, Transition-metal-based chalcogenides: A rich source of infrared nonlinear optical materials, *Coord. Chem. Rev.*, 2021, **448**, 214154–214192.

42 M. M. Chen, S. H. Zhou, W. B. Wei, X. T. Wu and Q. L. Zhu, Phase Matchability Transformation in the Infrared Nonlinear Optical Materials with Diamond-Like Frameworks, *Adv. Opt. Mater.*, 2021, **10**, 2102123–2102131.

43 O. V. Dolomanov, L. J. Bourhis, R. J. Gildea, J. A. K. Howard and H. Puschmann, OLEX2: A Complete Structure Solution, Refinement and Analysis Program, *J. Appl. Crystallogr.*, 2009, **42**, 339–341.

44 (*a*) W. W. Wendlandt and H. G. Hecht, *Reflectance pectroscopy*, Interscience Publishers, New York, 1966; (*b*) G. Kortüm, *Reflectance Spectroscopy*, Springer, 1969.

45 S. J. Clark, M. D. Segall, C. J. Pickard, P. J. Hasnip, M. I. Probert, K. Refson and M. C. Payne, First Principles Methods Using CASTEP, *Z. Kristallogr. – Cryst. Mater.*, 2005, **220**, 567–570.

46 Y. Chi, Z. D. Sun, Q. T. Xu, H. G. Xue and S. P. Guo, Hexagonal In_2Se_3: A Defect Wurtzite-Type Infrared Nonlinear Optical Material with Moderate Birefringence Contributed by Unique $InSe_5$ Unit, *ACS Appl. Mater. Interfaces*, 2020, **12**, 17711–17717.

47 Q. T. Xu, Y. Chi, X. H. Li, W. L. Liu and S. P. Guo, Structural Chemistry and Excellent Nonlinear Optical Properties of a Series of Ternary Selenides $Ga_x,In_{2-x}Se_3$, *Inorg. Chem.*, 2021, **61**, 431–438.

48 W. L. Yin, A. K. Iyer, X. Lin, C. Li, J. Y. Yao and A. Mar, A. Quaternary Chalcogenides $BaRE_2In_2Ch_7$ (RE = La-Nd; Ch =

S, Se) Containing $InCh_5$ Trigonal Bipyramids, *Dalton Trans.*, 2016, **45**, 12329–12337.

49 A. Rothenberger, H. H. Wang, D. Chung and M. G. Kanatzidis, Structural Diversity by Mixing Chalcogen Atoms in the Chalcophosphate System K/In/P/Q (Q = S, Se), *Inorg. Chem.*, 2010, **49**, 1144–1151.

50 I. Tiritiris and T. Schleid, The Crystal Structure of Solvent-Free Silver Dodecachloro-*closo*-Dodecaborate $Ag_2[B_{12}Cl_{12}]$ from Aqueous Solution, *Z. Anorg. Allg. Chem.*, 2003, **629**, 581–583.

51 B. W. Liu, X. M. Jiang, H. Y. Zeng and G. C. Guo, $[ABa_2Cl][Ga_4S_8]$ (A = Rb, Cs): Wide-Spectrum Nonlinear Optical Materials Obtained by Polycation-Substitution-Induced Nonlinear Optical (NLO)-Functional Motif Ordering, *J. Am. Chem. Soc.*, 2020, **142**, 10641–10645.

52 Z. T. Lu, Z. D. Sun, Y. Chi, H. G. Xue and S. P. Guo, Balanced Second-Order Nonlinear Optical Properties of Adducts $CHI_3{\cdot}(S_8)_3$ and $AsI_3{\cdot}(S_8)_3$: A Systematic Survey, *Inorg. Chem.*, 2019, **58**, 4619–4625.

53 B. W. Liu, H. Y. Zeng, X. M. Jiang, G. E. Wang, S. F. Li, L. Xu and G. C. Guo, $[A_3X][Ga_3PS_8]$ (A = K, Rb; X = Cl, Br): Promising IR Non-Linear Optical Materials Exhibiting Concurrently Strong Second-Harmonic Generation and High Laser Induced Damage Thresholds, *Chem. Sci.*, 2016, **7**, 6273–6277.

54 J. N. Li, W. D. Yao, X. H. Li, W. L. Liu, H. G. Xue and S. P. Guo, A Novel Promising Infrared Nonlinear Optical Selenide $KAg_3Ga_8Se_{14}$ Designed from Benchmark $AgGaQ_2$ (Q = S, Se), *Chem. Commun.*, 2021, **57**, 1109–1112.